

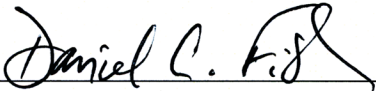
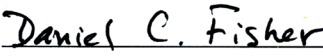
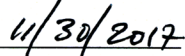
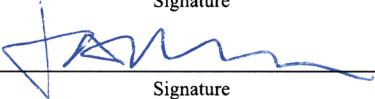
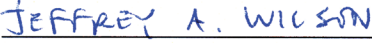

Joseph J. El Adli

Season of death of the Bowser Road mastodon

Submitted for Publication in:

Archaeological Recovery of the Bowser Road Mastodon Orange County, New York

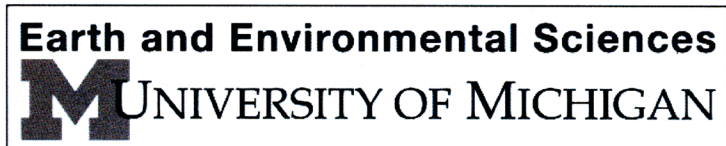
in lieu of thesis in partial fulfillment of the requirements for the degree of
Master of Science in Earth and Environmental Sciences
Department of Earth and Environmental Sciences
The University of Michigan

| | | |
|---|--|--|
|  Signature | Accepted by:  Name |  Date |
|  Signature |  Name |  Date |
| _____ Department Chair Signature | _____ Name | _____ Date |

I hereby grant the University of Michigan, its heirs and assigns, the non-exclusive right to reproduce and distribute single copies of my thesis, in whole or in part, in any format. I represent and warrant to the University of Michigan that the thesis is an original work, does not infringe or violate any rights of others, and that I make these grants as the sole owner of the rights to my thesis. I understand that I will not receive royalties for any reproduction of this thesis.

- Permission granted.
- Permission granted to copy after: _____
- Permission declined.

Author Signature



Season of death of the Bowser Road mastodon¹

ABSTRACT

A sample of dentin and cementum removed from the growing end of the left tusk of the Bowser Road mastodon was analyzed to document structural variation and interpret season of death for this individual. Within this tusk sample, we investigated three different patterns of structural variation: repeated step-wise changes in X-ray attenuation of dentin along transects perpendicular to the surface of the tusk pulp cavity (the surface of dentin apposition), highly variable but roughly cyclical variation in the thickness of structural increments of dentin (again measured normal to the surface of the pulp cavity), and topographic features expressed on the external surface of the tusk, encircling its root and paralleling its proximal margin. These three patterns of structural variation are linked in that each is initially manifested in dentin, and each occurs over a spatial scale determined by annual rates of dentin apposition and tusk extension. Based on previously documented associations between the structural features observed here and individual seasons comprising the annual cycle, we treat our annual increments as extending from one winter-spring boundary to the next. We also confirm that the structural increments for which we document the pattern of thickness variation formed

¹ El Adli, J.J.; Fisher, D.C.; DeLancey, L.C.; and Beld, S.G. 2017. Appendix IV: Season of death of the Bowser Road mastodon. *Archaeological Recovery of the Bowser Road Mastodon Orange County, New York*. Ed: Gramly, R.M. Persimmon Press, Massachusetts

periodically, spanning intervals of about one fortnight (two weeks) each. In a transverse thin section from a position near the middle of our sample slab, we observed two complete years of growth and a final interval of fifteen fortnights. This implies an early autumn season of death for the Bowser Road mastodon. In prior work, autumn deaths were probabilistically associated with active hunting by humans.

INTRODUCTION

Interpretation of any archaeological or paleontological site ultimately hinges on what new information can be extracted from specimens preserved at the site. Other parts of this monograph and its appendices describe the partial remains of an American mastodon (*Mammut americanum*) from the Bowser Road site and many aspects of its geological context. In this Appendix, our charge is to add several points of information that might at first seem insignificant but that could enhance our understanding of this site in unexpected ways. Foremost among these new details is the season of the year when this mastodon died. Prior studies (e.g., Fisher, 1987) have argued that there is at least a probabilistic association between season of death and cause of death for late Pleistocene proboscideans. In addition to our interest in the season of death for the Bowser Road mastodon, we recognize that success in resolving season of death might yield insights into tusk growth rates and other evidence of the animal's condition prior to death or aspects of the environment in which it lived.

In support of our study, a sample of tusk material from the Bowser Road mastodon was made available. Tusks are the large and continuously-growing incisors present in many proboscidean taxa. As with almost all teeth, when they are first formed, tusks are capped with a layer of enamel (located at the tusk tip, but usually worn away as the tusk is subjected to abrasion). However, the primary tissue that makes up the internal portion of the tusk is dentin. This grows by apposition at the conical pulp cavity surface near the basal, or proximal, end of the tusk. Previous studies have identified periodically-forming structural increments within tusks that allow interpretation of annual and subannual growth (Fisher, 1987; 1996; 2001). Similar growth features have been

documented in a variety of other mammalian teeth (Laws, 1952; Dean, 1987), but the ever-growing nature of tusks creates a potentially continuous record of growth from throughout most of an individual's life.

Fisher (1987; 2001) documented sets of hierarchically organized growth increments within tusk dentin. These form on daily (third-order increments), fortnightly (second-order, or two-week, increments), and yearly (first-order increments) intervals in tusks of *Mammot americanum* from North America. Appositional increments (those formed by processes of addition of new dentin along the surface of the pulp cavity) vary in thickness based on the quality and quantity of nutrient intake during (and probably prior to) the time of increment formation. During times of hardship, increments are expected to be thinner, but they are thicker during times of plenty. This leads to intra-annual variation in increment thickness related to seasonality and certain aspects of life history (schedules of growth and maturation) and inter-annual variation in increment thickness related to longer-term patterns of climate variation and other aspects of life history (e.g., Fisher, 2008; Fisher et al., 2008). Extensional increments (those formed by processes responsible for increase in tusk length) display a similar hierarchy of increment types, although third-order (daily) extensional increments have not yet been documented in proboscidean dentin.

The growth features we focus on here are all fundamental features of tusk dentin. They include patterns of appositional variation in X-ray attenuation (probably controlled mostly by density of mineralization), patterns of variation in thickness of second-order appositional increments, and locations of first-order extensional features. Coordinated analysis of these three sources of data will be used to identify annual increments of tusk

growth. Focusing then on the last (partial) year of life, we will infer season of death for the Bowser Road mastodon.

MATERIAL AND METHODS

The sample provided to us was cut from the proximal end of the left tusk. This tusk has a basal diameter of 16.5 cm and is associated with cheek teeth that include well-worn third molars and one heavily worn second molar (R. M. Gramly, pers. comm.). This combination of traits is typical for a mature male of moderately advanced age (Fisher, 2008). Based on the external surface curvature of our sample (convex in the transverse direction but concave in the longitudinal direction), it came from the inside curve, or dorsal aspect, of the tusk base. This region was chosen because it included some of the best-preserved dentin available, but most of our comparable analyses on other specimens have focused on samples from the outside curve, or ventral aspect, because equivalent increments are generally thicker and longer when measured on the outside curve, helping to minimize measurement error. Nevertheless, we have some measurements that allow us to treat observations on this specimen in a comparative context.

The entire tusk sample is about 5.5 cm wide (transversely) and 20 cm long. It is 3 cm thick at its distal end, from which it tapers proximally (following the conical wall of the pulp cavity) to about 1 mm in thickness near what originally would have been its extremely sharp growing margin. This sample is illustrated in **Figure 1**, where orthogonal views are organized according to the “box model” (as if projected through the faces of an enclosing box, which is then unfolded onto the page). Throughout this

sample, dentin and cementum were initially in contact along a two-dimensional surface located just inside the external surface of the tusk. This two-dimensional contact is the “dentin-cementum interface.” In contrast, when referring to the appearance of this contact as a one-dimensional feature in a cross-sectional view, we call it the “dentin-cementum junction”, or DCJ. At all points on our tusk sample, there is an essentially continuous sequence of dentin from the dentin-cementum interface to the pulp cavity surface. An extensive delamination fracture (a fracture that has propagated along an incremental feature) had formed over slightly more than the distal half of the tusk sample long before the sample was sent to us and possibly prior to excavation, but close inspection suggests there has been little or no loss of material along this fracture. The delamination fracture is located about 7.5 mm from the surface of the pulp cavity, and the dentin between it and the pulp cavity is relatively well preserved – hard and darkly stained by tannins. The dentin outboard of this fracture (between it and the cementum layer) is softer, lighter in color, and especially near the distal end of the sample, highly friable. Some of this friable dentin was lost during cutting the sample from the rest of the tusk (**Figure 1B, D**). Therefore, before any further modification, we consolidated this end of the sample by taping its edges, adding catalyzed epoxy resin to a reservoir at the distal end, and placing the entire specimen under a moderate vacuum to draw resin into fractures, after which the resin polymerized.

Having the size of specimen we did allowed some flexibility in choosing an area for detailed analysis, and it provided a good sample of the external tusk surface. However, the specimen was wider than would fit on a petrographic microscope slide for thin section production, and it was wider and longer than would fit into the sample

chamber of the microCT scanner to which we had access. We therefore cut a smaller block out of the larger sample, using an abrasive cut-off disk, a coping saw, and a carbide bit in a handheld rotary tool. The smaller block was approximately rectangular in outline and measured 7.5 cm long by 2 cm wide; it tapers in thickness from 2.3 cm thick distally to 1.2 cm proximally (**Figure 2**).

Before any modification of the small sample block, it was analyzed using X-ray computed microtomography (microCT) at the University of Michigan School of Dentistry, using a SCANCO Medical μ CT100 operating at 90kV, 78 μ A, and 500 ms, yielding uniform cubic voxels 60 μ m on each side. The sample was then visualized using Amira 5.4.1, which showed variations in X-ray attenuation within the tusk.

After CT-scanning and processing the scan data, we chose a location for a thin section where the density structure of the dentin seemed to be well organized. This location was near the middle of the small sample block. After marking the block at this position, it was cut transversely (perpendicular to the inclined pulp cavity surface) with a low-speed diamond wafering blade on a Buehler Isomet saw. One of the two resulting smaller blocks was cut a second time, parallel to the first, yielding a 6 mm-thick slab that was reserved for later analysis of stable isotope composition (not included in this study). The freshly exposed face of the other cut block (at the position selected by microCT analysis) was polished with 600-grit tungsten carbide abrasive paper and glued to a petrographic microscope slide with optical-grade epoxy resin. After polymerization, excess sample material was cut from the slide with the Isomet, and the remaining sample on the slide was polished through a range of grits, ending with a thickness that permitted adequate transmission of light (ca. 25 μ m). The finished thin section was

viewed after adding kerosene to its uncovered sample surface to increase light transmission and enhance increment visibility. The thin section was photomicrographed in plane-polarized light at 40x magnification using a Leitz petrographic microscope and a Canon 60D camera with a 50 mm Zeiss lens. Ten overlapping transects spanned the dentin sequence from the dentin-cementum junction to the pulp cavity. After calibration with a stage micrometer, the ImageJ (Rasband, 1997) plug-in IncMeas 1.3c (Rountrey, 2009) was used to measure the thickness of dentin increments in photomicrographs.

Interpretation of the pattern of variation in second-order increment thickness ultimately required us to go back to the microCT data and more closely investigate the pattern of variation in X-ray attenuation at the proximal end of the small sample block, beyond the proximal-most extent of the delamination fracture. In addition, we tested elements of our interpretation by tracing first-order extensional features on the external surface of the tusk sample and in cross-sectional views of the dentin-cementum junction. Documentation of some of these details required part of the longitudinally cut surface of the original tusk sample to be polished (using dry abrasive papers) to reveal the configuration of the dentin-cementum junction.

RESULTS

MicroCT

MicroCT provides a means of documenting variation in X-ray attenuation, most of which probably results from variation in density of mineralization. Transitions in attenuation within tusk dentin have been used in several previous studies to identify

annual appositional increments (Fisher et al., 2014; El Adli et al., 2015; 2016), and we thus undertook to assess the pattern of variation in this specimen, shown here in **Figure 3**. We note first that the circular pattern of luminance variation centered on a point near the upper right corner of **Figure 3A** is a “circular artifact” produced by the SCANCO’s algorithm for reconstructing the spatial pattern of variation in attenuation. Knowing that such a pattern is likely to emerge in the data, the user needs to orient the sample so that anticipated patterns of real variation in attenuation can be distinguished from this artifact. In our case, we expect temporal variation in attenuation recorded during the process of dentin apposition to be manifested as a series of zones paralleling the surface of the pulp cavity and forming a stacked series of features crossing the virtual section.

A further requirement for interpreting this record is to establish which part of the virtual section represents cementum and which part represents dentin. For this, we need not resort to speculation, because our thin section, shown here as **Figure 4**, comes from nearly the same position recorded by the virtual section, and the histological detail evident in this thin section makes the identity of each tissue unambiguous. As in the longitudinal sections seen in **Figure 1B** and **D**, the cementum layer is darker-colored than adjacent dentin and lacks both fine-scale incremental features and evidence of dentinal tubules. Across the top of the section illustrated in **Figure 4**, the cementum layer varies irregularly from about 1.5 mm to about 2.5 mm in thickness. Once the extent of cementum in **Figure 3A** is recognized (if necessary by copying the trace of the DCJ from **Figure 4** to **Figure 3A**), it becomes clear that the bright zone along the external surface of the tusk in **Figure 3A** is only the uppermost

portion of the cementum. Below this is a zone of lower luminance and below that, a reversion to a thin zone of higher luminance (or higher attenuation). The thin zone of low attenuation that comes next probably reflects a thin, lightly mineralized zone of dentin that is normally found just inside the DCJ, and as such, it may not have temporal significance; like the DCJ itself, this would be a time-transgressive boundary.

Further insight into these patterns can be gained by checking the virtual section in **Figure 3B**, taken near the proximal end of the smaller block of dentin (**Figure 2**) cut from the larger tusk sample. The circular artifact has a different center point here because the sample block was intentionally tilted within the sample carrier, so that an inauspicious conjunction of artifact and feature in one virtual section might be avoided in another. The position of the DCJ marked at the upper right in **Figure 3B** was verified on the specimen. Just to the left of the DCJ arrow in **Figure 3B** is an air-filled gap where differential shrinkage (associated with desiccation) of cementum and dentin has resulted in spalling along this interface. Moving toward the center and left portion of this virtual section, there is also delamination within the cementum sequence, which “grows” by apposition of layers from the DCJ outward. In terms of variation in attenuation, we see a similar sequence of cementum layers here to the sequence observed in **Figure 3A**, although the total thickness, and possibly the thickness of individual layers, is less than in **Figure 3A**.

Other features of the virtual sections in **Figure 3** are radially oriented tension fractures that appear as epoxy-filled (black, zero luminance) gaps in the upper left of each image. These form as dentin (and to a lesser degree cementum) shrinks during desiccation and contracts transversely. The longitudinal continuation of these features

shows up in a similar position in **Figure 3B**. In each case, these fractures terminate at, and thus must postdate, the delamination fracture (also epoxy-filled) that parallels the pulp cavity surface roughly midway through the section. An additional tension fracture in **Figure 3A**, just to the left of the center of the circular artifact, is radially oriented within the dentin but then turns to follow the DCJ; this fracture does not extend longitudinally to the position of **Figure 3B**.

Turning now to the dentin sequence in **Figure 3A**, we see a series of mostly subtle step-wise changes in attenuation that are labeled along the left margin of the virtual section. This pattern is more complex than we might have expected, and at first glance, there is no clear sign of a repeating pattern that might indicate an annual cycle. Just inside the DCJ is a zone of high attenuation for which we have no clear beginning (since earlier-formed dentin would only be found in a more distal position on the tusk). However, this zone ends at a point corresponding to the tip of the arrow associated with the half-bracket labeled *a*. Moving in the direction of dentin apposition, we next encounter a zone of lower attenuation that we leave unmarked, followed by a wider zone of higher attenuation for which the beginning and end are marked by the tips of the arrows associated with bracket *b*. In similar fashion, with intervening unmarked zones of lower attenuation, we label high-attenuation zones *c*, *d*, and *e*. Zone *d* requires some comment, in that it is interrupted by the delamination fracture. We marked this as one zone rather than two because there was no apparent change in attenuation adjacent to the fracture, but we reserve further interpretation of this feature for the Discussion below. Each of the zones labeled *b*-*e* has parallel boundaries that extend conformably and without interruption (except for their intersection with the circular artifact) across the

virtual section. It is thus plausible that they represent a time-series of shifts in the intensity of dentin mineralization. We left the final high-attenuation zone adjacent to the pulp cavity unmarked because we often see a high-attenuation zone in this position and suspect that it forms secondarily, during diagenesis, as a result of interaction between the dentin near this exposed surface and pore waters associated with sediment filling the pulp cavity (Fisher et al., 2014; El Adli et al., 2015; 2016).

A similar account of **Figure 3B** begins with a high-attenuation zone for which we have only the termination, marked by the tip of the arrow associated with half-bracket b' . As above, we then encounter high-attenuation zones labeled c' , d' , and e' , except that between d' and e' , there is another high-attenuation zone labeled z . As above, we do not label the high-attenuation zone next to the pulp cavity.

Thin Section

As noted above, the thin section illustrated in **Figure 4** comes from the same location as the virtual microCT section in **Figure 3A**. Unlike some dentin sequences we have studied (e.g., Fisher, 1987; 2008), there was no clear first-order (annual) pattern of variation in color – usually a dark zone in close association, often just before, what we recognize as a winter-spring boundary. Instead, the dentin in this thin section shows very little color modulation throughout its thickness. However, dark-light couplets that we recognize as having the scale and character of second-order (fortnightly) appositional increments are clearly developed in most parts of the sequence. These features are all conformable to one another (they do not cross or otherwise intersect), and all parallel the surface of the pulp cavity. We found these features to be best

preserved along the right edge of **Figure 4**, so our photomicrographs followed this margin.

Our confidence that we were dealing with second-order increments was increased by discovery that in some parts of the thin section, third-order, or daily, dentin increments were also observable. In addition to being characterized by histological features discussed previously (Fisher, 1987), these show a relatively constant numerical relation to second-order increments. In tusk dentin of *Mammut*, there are usually 14 third-order increments within each second-order increment. In our thin section, we saw this best in a succession of increments shown in **Figure 5**. The third-order increments shown here are faint, but easy to count in scattered patches and possible to distinguish more or less throughout the sequence. The second-order increment boundaries are somewhat harder to localize in this image, because of their scale, but they show up better if traced across a broader lateral extent. One complication in documenting this pattern is that there is often a somewhat darker zone about midway between what we take to be second-order increment boundaries. When these are clearly subsidiary features and when the third-order increments are clear enough to count, we can generally identify the boundaries of interest. However, in transects where third-order increments are obscure, it is always possible that an extra second-order increment boundary could be identified (or one missed) with the expected consequences for the pattern of sequential increment thicknesses (resulting in additional, but thinner increments or fewer, but thicker increments).

Second-order dentin increments are attributed a thickness equal to one wavelength in their cycle of luminance variation (i.e., one complete dark-light couplet).

In principle, this cycle could be treated as beginning at any convenient point, but since the dark phases of the cycle tend to be narrower and more discrete, we measure from the middle of one dark phase to the next. Each increment is thus bounded by a dark feature, and each of these features is numbered, starting with 0 at the DCJ. The thickness of the increment between features 0 and 1 is then plotted and assigned arbitrarily to “increment 1”, followed by increments 2-77 on the graph in **Figure 6**. The black line connecting points on this graph shows the pattern of variation in increment thickness, and the gray line shows a five-point moving average over the original data. Full second-order increments appeared to precede (increment 40) and follow (increment 41) the delamination fracture near the middle of this sequence. This fracture thus does not “interrupt” the graph but is noted at increment 40. Time runs from the DCJ at left to the surface of the pulp cavity at right, where the last increment thickness, marked with a dagger symbol, corresponds to dentin apposition just before death.

First-order Extensional Increments

A third source of information on the temporal scale of processes of tusk growth involves first-order extensional increments. These are typically bounded distally and proximally by positive topographic features, or ridges, for which the term “periradicular bands” has been used (e.g., Fisher, 2008; El Adli et al., 2015). Near the proximal margin, these may be evident even on the outer surface of the cementum, but when present, they always turn out to originate at the dentin-cementum interface as an abrupt deflection of this contact. As cementum is added over a given feature, draping original relief, the external aspect of the feature becomes more and more subdued. However, a

longitudinal section through the cementum will generally allow the feature to be identified. The deflection of the dentin-cementum interface may take different forms, not all of which are well understood, but it is generally a relatively localized feature, separated from preceding and succeeding features by intervals of lower relief in the longitudinal direction.

The expression of periradicular bands on the external surface of our tusk sample is shown by white dashed lines in **Figure 1A**. Most of these features show clear relief near the upper border of this image, but then lose much of this relief as they are traced toward the lower border. The deflection of the dentin-cementum interface underlying most of these features is hinted at by tracing the DCJ near the lower border of the image in **Figure 1D**, where periradicular features are marked by asterisks (one of which is placed in parentheses because it is too subtle to be securely located along this edge of the specimen). A larger magnification view of the first of these features to form, located near the lower right corner of **Figure 1D**, is provided in **Figure 7**.

An additional part of the system of extensional features is shown near the lower left border of the image in **Figure 1A** (and again near its upper border), where cementum has spalled off, revealing second-order extensional features manifested as dentin color bands that parallel the proximal margin of the tusk as they cross the dentin-cementum interface. These are understood as the extensional representation of the same features identified as bounding second-order appositional increments. If more cementum had spalled off, these color bands would have been useful for corroborating recognition of first-order extensional features, but too few of them are currently exposed for this application.

DISCUSSION

If each of the data sources we investigate here had worked out as in a “best case scenario”, there would be little need for discussion and weighing of alternatives. However, for reasons that may become more clear as we proceed, the signal of changing seasons in the last years of life for this individual is not as clear as in many cases we have studied previously (Fisher, 1987; 2001; 2008; Fisher and Fox, 2003; Fisher et al., 2014; El Adli et al., 2016). We therefore begin this analysis by discussing extensional features, as they seem to have provided the clearest result.

Using extensional features to address the issues we hope to resolve in this analysis can be handled in two ways. The first presumes that first-order extensional features only show the scale of annual increments in tusk length. This still offers a critical constraint on interpretation of the rest of the tusk sample, including the full range of oppositional features. Accepting the periradicular features marked by white dashes in **Figure 1A** as annual increment boundaries – and the only such boundaries to be found on this part of the specimen – implies that there are two complete years, labeled X-1 and X-2, between the proximal margin and the location of our thin section. In addition, an unknown interval of less than one year is represented between the proximal-most periradicular feature and the proximal margin. We call this year X because we do not have a precise estimate of the animal’s age during this year, and all other years are numbered relative to this last (partial) year of life. Another incomplete year must be present between the beginning of year X-2 and the location of the thin section. The entire thickness of dentin represented in the thin section must correspond to the entire

record of tusk extension between the position of the thin section and the proximal margin. Any event from an earlier part of this animal's life will have been recorded distal to the location of the thin section and thus will not be recoverable from this part of the record. Therefore, however we choose to interpret patterns of variation in X-ray attenuation in the virtual section and patterns of variation in second-order increment thickness in the thin section, we expect to find two complete years bracketed by two incomplete years.

A second and stronger form of this argument relies on the fact that the best-studied examples of periradicular features show not only a temporal periodicity of about one year, but a close association with one part of a year, the winter-spring boundary (e.g., Fisher 2008). If we accept this association, then both the virtual section and the thin section (both located at nearly the same position) must record roughly the winter of year X-3, all of years X-2 and X-1, and roughly half of year X, from its winter-spring boundary to approximately the beginning of autumn. With this as a working hypothesis, we now turn to our other sources of information.

Returning to patterns of variation in X-ray attenuation, where these have been best-studied thus far (Fisher et al., 2014; El Adli et al., 2015; 2016), we are used to seeing one cycle of rising and falling X-ray attenuation per year, with the rise typically gradual, usually during the winter, and the fall typically abrupt, occurring in close association with the winter-spring boundary. However, in another study currently in review, we see two cycles of rising and falling attenuation per year, with all changes relatively abrupt. Clearly, there is room for variation in the natural history of this trait. *A priori*, we know little about what to expect, except that there might be a consistent

pattern with relatively few cycles per year, and the spatial scale of an annual pattern should be compatible with precedents for rate of apposition.

As noted above, the delamination fracture near the middle of the dentin sequence in **Figures 3** and **4** appears to have formed before the radially oriented tension fractures. The latter could have formed post-excavation, but because all of the dentin between the DCJ and the delamination fracture is less well preserved than dentin between the delamination fracture and the pulp cavity, we suspect that the dentin in the outer portion of this sample has seen significant interaction with groundwater, which probably gained access via the delamination fracture. This scenario of diagenetic interactions raises the possibility that the high-attenuation zone straddling the delamination fracture is not part of the time-series of dentin mineralization at all, but a secondary alteration of the dentin on both sides of the delamination fracture analogous to the high-attenuation zone adjacent to the pulp cavity. The alternative – that a delamination fracture propagated precisely down the middle of a highly mineralized zone – seems improbable in terms of fracture physics. To test this hypothesis, we followed the delamination fracture and its associated high-attenuation zone *d* in **Figure 3A** all the way to the proximal end of the sample block removed for **Figure 2**. **Figure 3B** represents a transverse virtual section just before this point, where a narrow hint of the delamination fracture still persists, along with its associated high-attenuation zone *d'*. However, just beyond this, the fracture and zone *d'* fade out. In this part of the sample block, all of the dentin from the DCJ to the pulp cavity is similarly well preserved, and this is where we encountered a surprise – a new zone of high attenuation – faint, but relatively clear – here labeled *z*. Our hypothesis is that *z* was not evident more distally

on the tusk because of a more complex history of dentin interaction with groundwater moving along the delamination fracture, and that a more unaltered pattern of variation in attenuation was preserved in the proximal wedge of dentin beyond the influence of the delamination fracture.

Factoring out d and d' as secondary features, like high attenuation adjacent to the pulp cavity, and adding z to the overall picture, we now have the following sequence of high-attenuation zones in **Figures 1A** and **B**: a relatively thick zone b that could correlate with a zone of unknown thickness b' ; a relatively thin zone c that apparently correlates (both are located just outside of the delamination fracture) with a thin zone c' ; a relatively thick zone z (without a distinct correlate in **1A**); and a relatively thin zone e that apparently correlates with e' (given their similar relationship to the surface of the pulp cavity). “Thick-thin, thick-thin” seems like two repetitions of a two-element cycle, in a sequence where we expect two cycles, with an incomplete cycle before and another after. In fact, it is possible that the last zone before the pulp cavity includes part of a thick high-attenuation zone (an unlabeled and hypothetical f') that is masked by the mineralization along the pulp cavity. At the very least, the number of cycles seems comparable to what we expect based on first-order extensional features.

Can we do more? On the longitudinal section produced by the saw cut defining the upper margin of **Figure 1A**, it is possible to trace increments closely associated with the delamination fracture (just below the lower edge of c') to a position on the DCJ just beyond the first-order periradicular feature separating extensional years X-1 and X-2. Likewise, increments at about the position of the lower edge of e' can be traced to the first-order periradicular feature separating extensional years X and X-1. At minimum,

this corroborates a correlation between appositional and extensional years X-2, X-1, and X. If we in addition accept that first-order periradicular features are associated with winter-spring boundaries, then the lower edges of *c* and *c'* and *e* and *e'* also represent winter-spring boundaries, replicating in part the previously established association between winter-spring boundaries and an abrupt transition from high to low X-ray attenuation. The only non-standard element of this system is that each annual interval also involves a second, thicker zone of high attenuation, earlier in the year. As noted above, although not as well documented as the one-high-attenuation-zone-per-year pattern, the two-high-attenuation-zones-per-year pattern is not unprecedented.

It now remains to link first-order extensional features and patterns of variation in X-ray attenuation to the pattern of variation in thickness of second-order appositional increments shown in **Figure 6**. Reviewing our recent steps, first-order extensional increment boundaries (i.e., periradicular features) have been correlated with step-wise changes in X-ray attenuation, allowing us to distinguish features along the left margin of **Figure 3** that are indicative of annual appositional increment boundaries marked by arrows on the right side of **Figure 3**. These arrows have then been transferred to the center of **Figure 4**, along with the labels for the years they bound. The positions of these year boundaries can then be traced along individual second-order dentin increments, into the transects measured on our photomicrographs and thus linked to the increment thickness profile plotted in **Figure 6**. At this point, we have already provisionally identified parts of each annual cycle with seasons, but will the pattern of second-order increment thickness variation corroborate this interpretation?

The vertical dashed lines on **Figure 6** mark the annual appositional increment boundaries carried from earlier stages of this analysis (both extensional features and microCT), and we have provisionally identified them as winter-spring boundaries. The increments that precede the first of these boundaries (on the left in **Figure 6**) are thin, consistent with late winter, but they are also located near the DCJ, where previous work has demonstrated that all appositional increments within the first two years inside the DCJ experience some degree of thickness attenuation because newly differentiated odontoblasts take about this long to achieve their full rate of dentin apposition (Fisher, 2008; Fisher et al., 2008). Viewed in this light, the general rise in second-order increment thickness through years X-2 and X-1 probably reflects this trend, with only year X demonstrating a more nearly normal rate of apposition. Nonetheless, the pattern of thickness variation within year X-2, focusing on the five-point moving average to smooth out a fairly noisy signal, can be described as a rise through spring into summer, followed by a midsummer depression, a second rise in early autumn, and then a decline into winter. Year X-1 is more noisy than X-2 but is more or less similar, with a somewhat earlier run of thin increments in the summer. Year X shows an initial rise, a pronounced mid-summer decline, but following a brief recovery, a moderate decline toward the time of death, fifteen fortnightly increments past the winter-spring boundary, which corresponds to early autumn.

The two complete years in this record are each recognized as including 28 second-order increments, two more than expected in a normal year (with 26 fortnights). Although the conditions that herald spring can always occur late or early in any given year, leading to an excess or deficit of second-order increments, it is also possible that

we have misidentified one or more increments in our analysis of photomicrographs. The appositional thicknesses of these two years, 4.7 mm for X-2 and 5.5 mm for X-1, are thinner than expected for a healthy, mature male, but again, years this close to the DCJ will only be displayed at a fraction of the thickness observed for the same year, recorded by odontoblasts located farther from the DCJ (i.e., farther from the proximal margin of the tusk and farther into the depth of the pulp cavity). Translation of these thicknesses to match expectation for the outer curve of the tusk would represent a slight further increase (Fisher et al., 2008), but for an individual of advanced age, we do not expect years to be as thick or long as seen in younger animals. Overall, these year-records do not differ significantly from expectation, considering their proximity to the DCJ.

Midsummer declines in second-order increment thickness are the expected pattern in association with a musth episode (Poole and Moss, 1981), the hormonally-mediated period of intense mating activity, fasting, and thus reduced rates of dentin apposition. Summer is the time of year when musth is expected, for the 22-month gestation period characteristic of proboscideans to yield a calf born in the spring, with the best opportunity for growth before its first winter (Fisher, 2008). All aspects of this record appear to be consistent with the seasonal identifications elaborated thus far.

The “noisiness” of the second-order increment thickness profile could be a function of local climate, including proximity to the coastal zone with maritime conditions and low to moderate seasonality. Another apparent anomaly, the reversed relative magnitudes of first-order appositional increments and first-order extensional increments for years X-2 (4.4 cm long) and X-1 (2.6 cm long) is also an outcome that potentially

carries its own paleobiological signal. Rates of apposition have been hypothesized to reflect a balance of conditions emphasizing mineral intake, while rates of extension may reflect a balance of conditions emphasizing protein intake (Fisher 2001; 2008).

An autumn death places the Bowser Road mastodon within a suite of cases that are all, as far as we know, associated with evidence of human activity related to carcass processing (Fisher, 1987; 2009). It is of course possible that some, if not all, of these animals died of causes unrelated to human activity. For the Bowser Road mastodon in particular, death comes soon enough after the conclusion of an inferred musth interval that we cannot rule out causation by lingering effects of an injury sustained in a musth battle. For such cases, evidence of carcass processing implies human scavenging of natural deaths, but we cannot explain away all autumn deaths in this way without addressing a critical question. If all autumn deaths, most of which are adult males, are scavenged natural deaths, rather than hunted animals, why is it that no such deaths (within our sample) escaped scavenging by humans? In this sense, it becomes difficult to avoid the conclusion that some, and possibly many, of these autumn deaths are victims of human hunters. Additionally, autumn deaths will generally involve animals in good condition, having just come through the time of year with the most abundant food resources. Autumn is also the time of year when excess meat, fat, and other animal products can be most easily and reliably stored in sub-aqueous settings as a precaution against shortages that could develop during winter, with the likelihood of harsh conditions and reduced mobility (Fisher, 1995; 2009). Other times of year are also associated with characteristic agents of mortality, such as death as a consequence of severe weather events or birth of a calf in late winter or early spring, or death as a

consequence of a musth battle in early or middle summer. Ultimately, season of death rarely drives a simple deduction of the cause of death, but it can condition probabilistic constraints on the likelihoods of hypothesized causes.

CONCLUSIONS

Integrated analyses of microCT data on patterns of variation in X-ray attenuation in tusk dentin, thin section analysis of patterns of variation in second-order appositional increments in tusk dentin, and tracing of first-order extensional increments in tusk dentin establish the scale and seasonal attribution of annual features of tusk growth for the Bowser Road mastodon. Our observations lead us to conclude that this animal died in early autumn and that its death, though possibly influenced by earlier musth conflict, could also have been caused by hunting activity by humans. The amount of time to which this study gives us access is only on the order of three years, but our measurements are consistent with this being an animal of reasonably good health living in a generally favorable environment.

ACKNOWLEDGMENTS

We thank A. Rountrey for providing the plug-in Inc Meas 1.3C that was used in this study, and for discussions of results. M. Lynch assisted us in the microCT Core Facility at the University of Michigan Dental School. We are also grateful for Michael Gramly's invitation to work on this specimen, for arranging the loan of the tusk sample, and for providing tusk measurements and information on associated cheek teeth.

REFERENCES

- Dean, M.C., 1987. Growth layers and incremental markings in hard tissues, a review of the literature and some preliminary observations about enamel structure in *Paranthropus boisei*. *Journal of Human Evolution* 16, 157-172.
- El Adli, J.J., Cherney, M.D., Fisher, D.C., Harris, J.M., Farrell, A.B., Cox, S.M., 2015. Last years of life and season of death of a Columbian mammoth from Rancho La Brea. In: Harris, J.M. (Ed.), *La Brea and beyond: The paleontology of asphalt-preserved biotas*. Natural History Museum of Los Angeles County, Science Series vol 42, pp. 65–80.
- El Adli, J.J., Fisher, D.C., Vartanyan, S.L., Tikhonov, A.N. 2016. Final years of life and seasons of death of woolly mammoths from Wrangel Island and mainland Chukotka, Russian Federation. *Quaternary International*.
<http://dx.doi.org/10.1016/j.quaint.2016.07.017>
- Fisher, D.C., 1987. Mastodont procurement by Paleoindians of the Great Lakes Region: Hunting or scavenging? In: Nitecki, M.H., Nitecki, D.V. (Eds.), *The evolution of human hunting*. Plenum, New York, pp 309–421.
- Fisher, D.C., 1995. Experiments on subaqueous meat caching. *Curr Res Pleistocene* 12, 77–80.
- Fisher, D.C., 1996. Extinction of proboscideans in North America. In: Shoshani, J., Tassy, P. (Eds.), *The Proboscidea: Evolution and palaeoecology of elephants and their relatives*. Oxford University Press, Oxford, pp 296–315.

- Fisher, D.C., 2001. Season of death, growth rates, and life history of North American mammoths. In: West, D.L. (Ed.), *Mammoth site studies: Proceedings of the first international conference on mammoth site studies*. Publications in Anthropology vol. 22, University of Kansas, Lawrence, pp. 121–135.
- Fisher, D.C., 2008. Taphonomy and paleobiology of the Hyde Park mastodon. In: Allmon, W.D., Nester, P.L. (Eds.), *Mastodon paleobiology, taphonomy, and paleoenvironment in the late Pleistocene of New York State: Studies on the Hyde Park, Chemung, and Java sites*. *Palaeontographica Americana* vol. 61, pp. 197–289.
- Fisher, D.C., 2009. Paleobiology and extinction of proboscideans in the Great Lakes region of North America. In: Haynes, G. (Ed.), *American megafaunal extinctions at the end of the Pleistocene*, Springer, New York, pp. 55–75.
- Fisher, D.C., Beld, S.G., Rountrey, A.N., 2008. Tusk record of the North Java mastodon. In: Allmon, W.D., Nester, P.L. (Eds.), *Mastodon paleobiology, taphonomy, and paleoenvironment in the late Pleistocene of New York State: Studies on the Hyde Park, Chemung, and Java sites*. *Palaeontographica Americana* vol. 61, pp. 417–463.
- Fisher, D.C., Cherney, M.D., Newton, C., Rountrey A.N., Calamari, Z.T., Stucky, R.K., Lucking, C., Petrie, L., 2014. Taxonomic overview and tusk growth analyses of Ziegler Reservoir proboscideans. *Quaternary Research* 82, 518–532.
- Fisher, D.C., Fox, D.L., 2003. Season of death and terminal growth histories of Hiscock mastodons. In: Laub, R., Miller, N., Steadman, D. (Eds.), *The Hiscock Site: Late*

Pleistocene and Holocene paleoecology and archaeology of western New York State, Bulletin of the Buffalo Society of Natural History vol. 37, Buffalo, New York, pp. 83–101.

Fox, D.L., Fisher, D.C., 1994. Tusk growth rate in *Loxodonta africana* as recorded by incremental laminae in tusk dentin. *Journal of Vertebrate Paleontology* 14, 26A

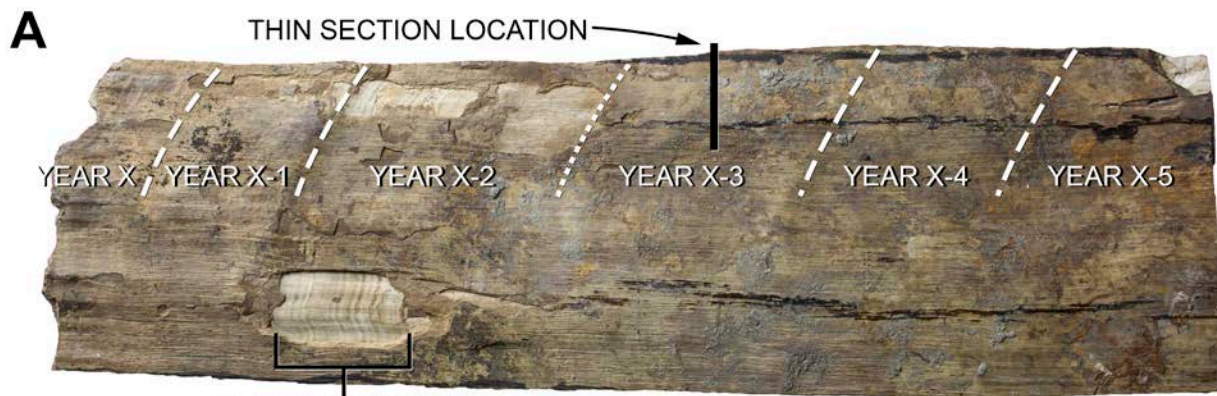
Laws, R.M., 1952. A new method of age determination for mammals. *Nature* 169, 972.

Poole, J.H., Moss, C.J., 1981. Musth in the African elephant, *Loxodonta africana*. *Nature* 292, 830–831.

Rasband, W.S., 1997. ImageJ. United States National Institutes of Health, Bethesda, Maryland. <http://imagej.nih.gov/ij/>.

Rountrey, A.N., 2009. Life histories of juvenile woolly mammoths from Siberia: Stable isotope and elemental analyses of tooth dentin. Ph.D. dissertation, University of Michigan, xiii+331 pp.

Figure 1. Sample from the proximal (growing) end of the left tusk of the Bowser Road mastodon. A, Outer surface of tusk, covered mostly by cementum; proximal margin at left; transversely cut distal margin at right; longitudinal cuts on upper and lower margins; vertical black bar shows location of transverse thin section; white dashed curves show locations of first-order (annual) periradicular features, with years identified between them; small bracketed region at lower left reveals dentin-cementum interface with second-order (fortnightly) periradicular features visible where cementum has spalled away. B. Longitudinal section formed by cut at lower margin of A; external tusk surface (mostly cementum, dark in cross section) along uppermost edge; pulp cavity situated below this part of specimen. C. Direct view of pulp cavity surface; proximal margin at left; distal cut at right; longitudinal cuts on upper and lower margins. D. Longitudinal section formed by cut at lower margin of C; pulp cavity situated above this part of specimen; external tusk surface (mostly cementum, dark in cross section) along lowermost edge; asterisks mark locations of first-order (annual) periradicular features defined by a deflection of the dentin-cementum interface; middle asterisk (in parentheses) less pronounced than others. Scale bar applies to A-D.



2° PERIRADICULAR BANDS

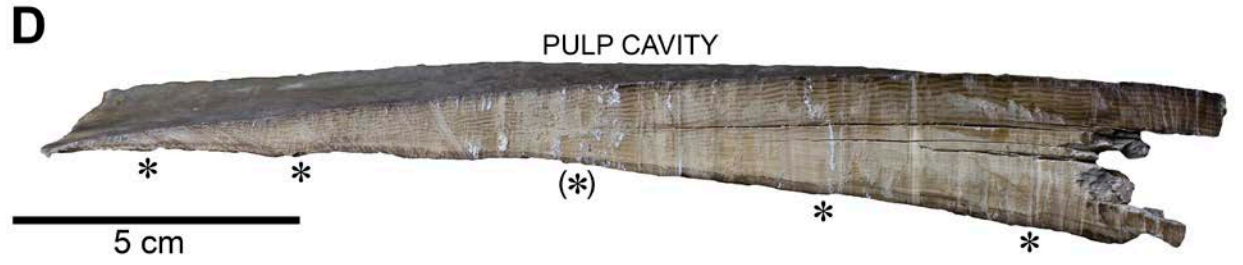
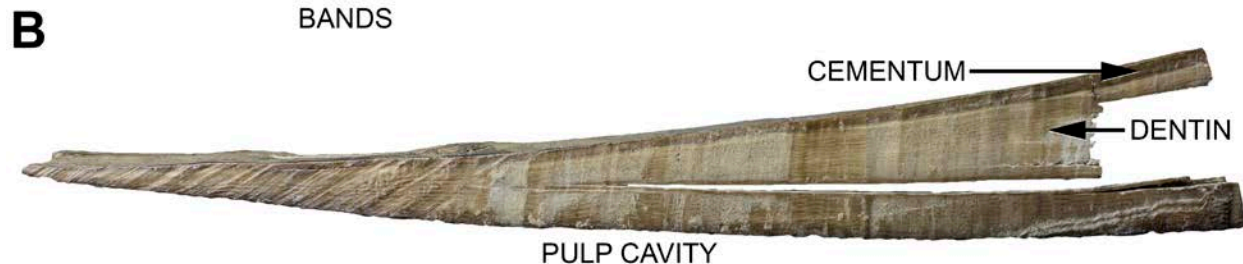


Figure 2. Original sample of Bowser Road mastodon tusk after removal of smaller sample for analysis by microCT and thin section.

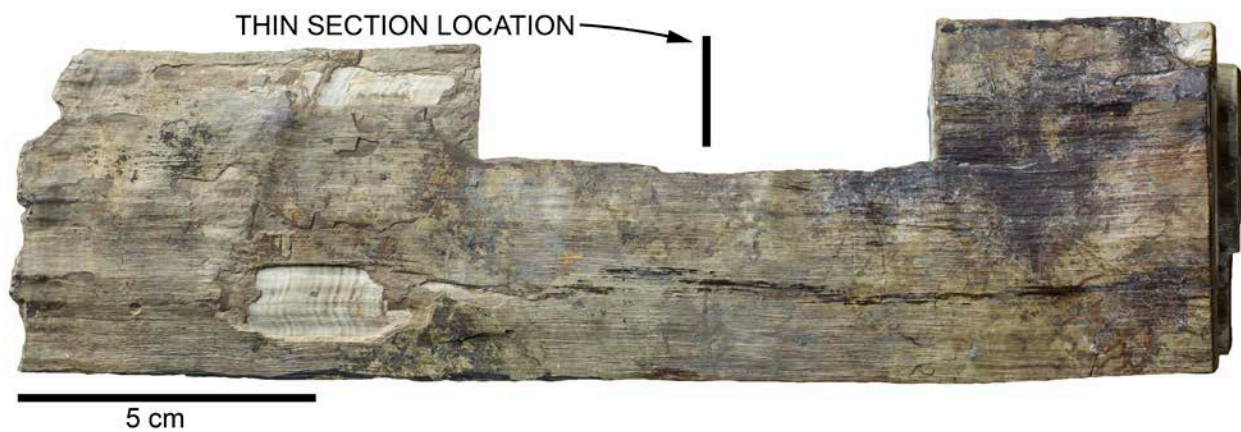


Figure 3. Transverse virtual sections showing microCT data measuring variation in X-ray attenuation of tusk tissues. A. Virtual section adjacent to thin section located at the position of the vertical black line in Fig. 1A; lettered brackets and arrows at left mark beginnings and ends of zones of elevated attenuation (higher luminance) within dentin; arrows at right mark DCJ (dentin-cementum junction) and inferred winter-spring boundaries separating years X-2, X-1, and X. B. Virtual section located ca. 3.8 cm from thin section location, in the proximal direction; lettered brackets and arrows at left mark beginnings and ends of zones of elevated attenuation; arrows at right mark DCJ and inferred winter-spring boundaries separating years X-1 and X. Scale bar applies to A-B.

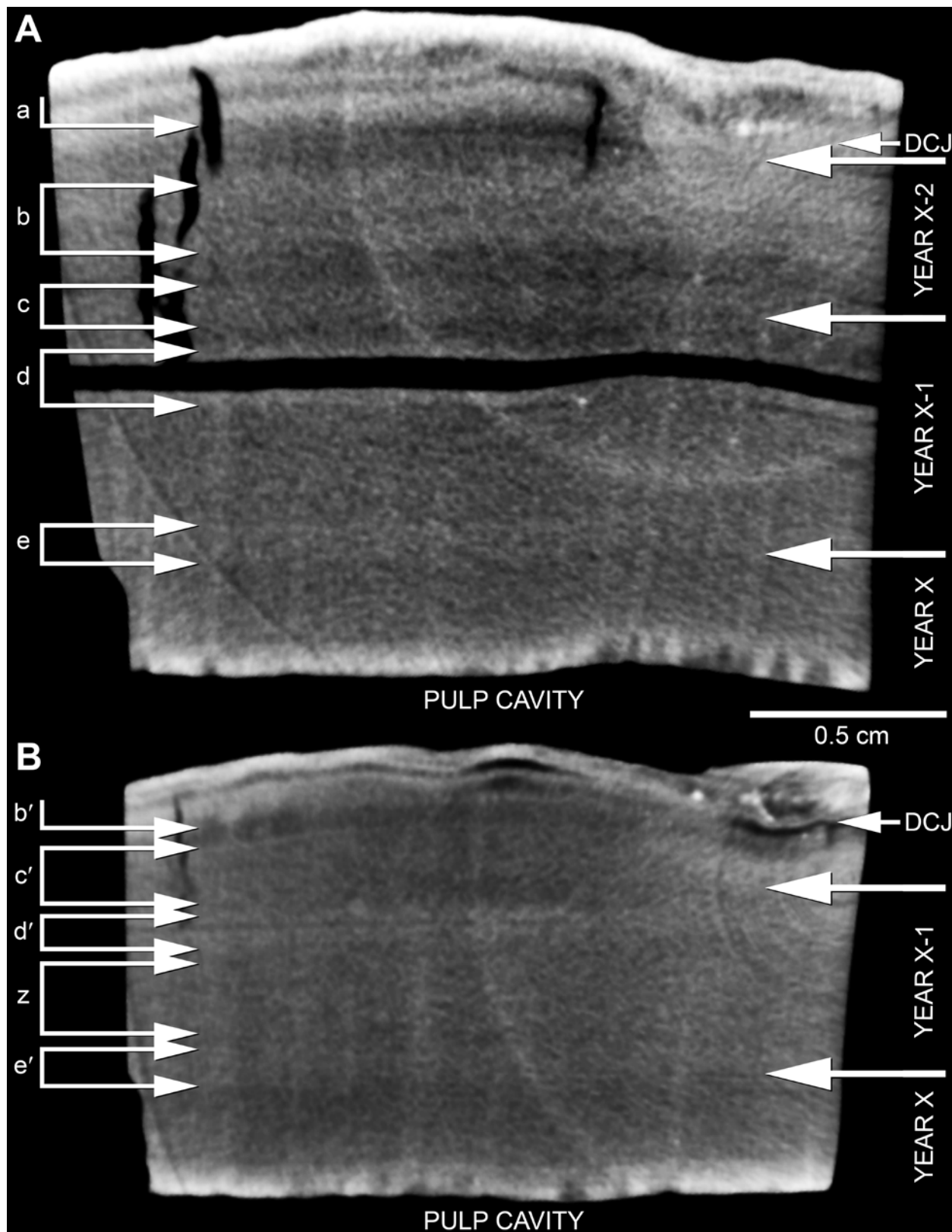


Figure 4. Photomicrograph of transverse thin section located at the position of the vertical black line in Fig. 1A. Dark layer forming outer surface of specimen (at top of image) is cementum. Dentin is lighter-colored material extending from just below cementum to the surface of the pulp cavity (at bottom of image). DCJ (dentin-cementum junction) is not perfectly conformable to incremental features in dentin. Arrows and brackets near middle of image mark positions of winter-spring boundaries transferred from right margin of Fig. 2A. White lines trace individual second-order increment boundaries from arrows marking inferred winter-spring boundaries toward the right, into higher magnification photomicrographs recording transects used for measuring thicknesses of second-order dentin increments. Scale bar at lower left.

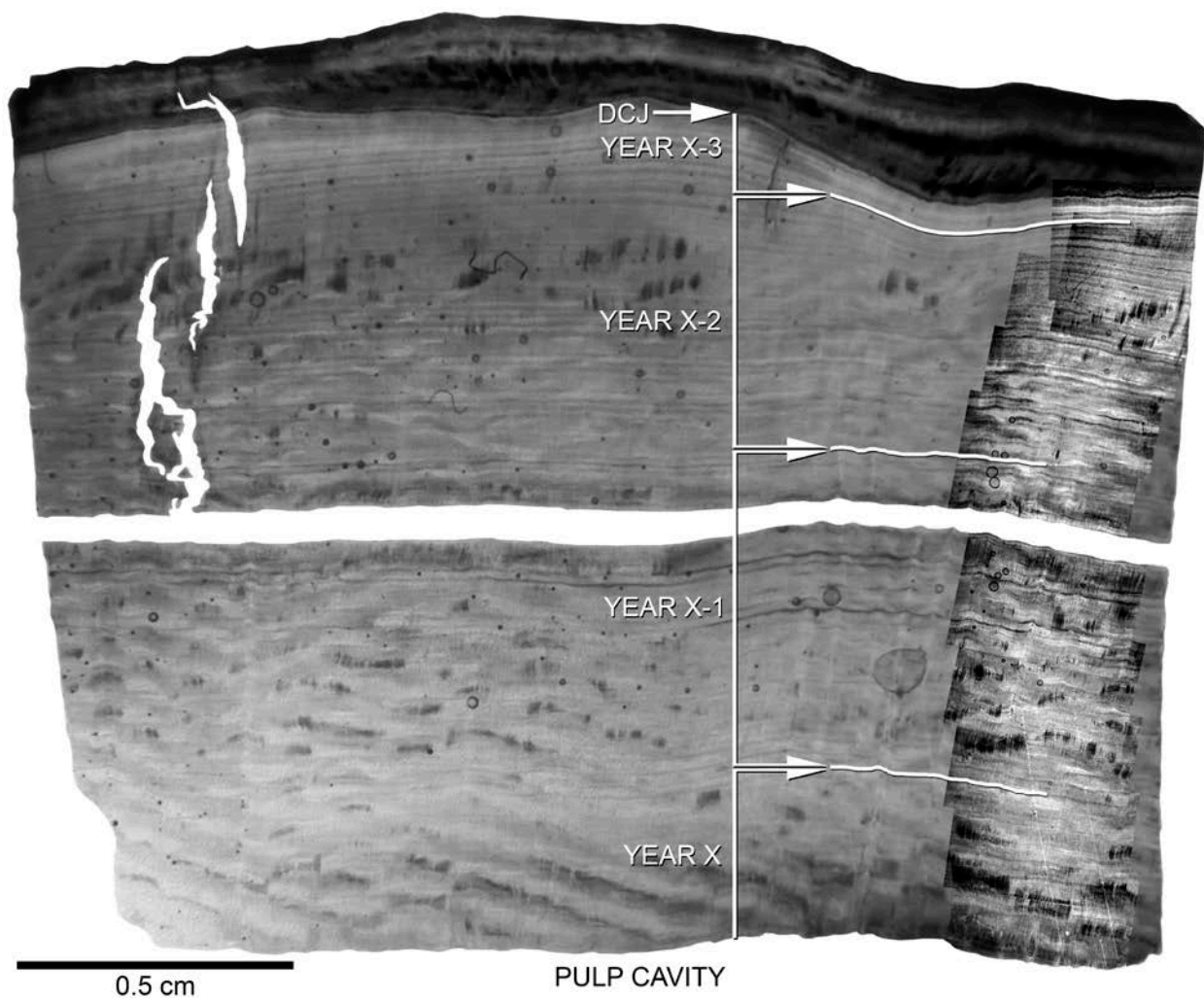


Figure 5. Photomicrograph of a series of second-order (fortnightly) dentin increments spanning a zone where third-order (daily) increments can also be seen. There are 14 third-order increments within each second-order increment. This image is cropped from transect 8, and the three second-order increments are bounded by numbered incremental features 58, 59, 60, and 61. Scale at lower right of image.

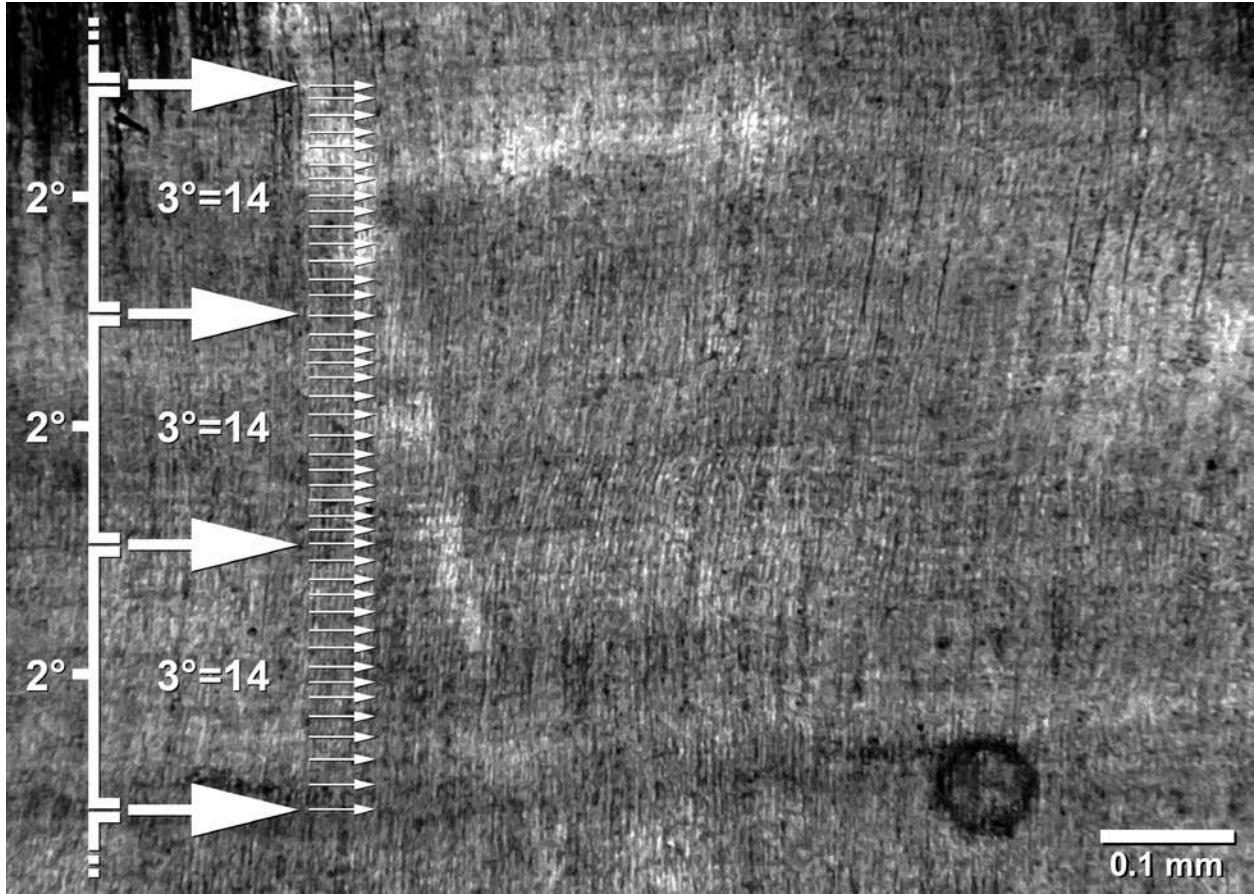


Figure 6. Graph of second-order increment thicknesses vs. distance from the pulp cavity measured on the thin section located at the position of the vertical black line in Fig. 1A. Every tenth increment boundary is numbered from left (DCJ) to right (pulp cavity). Year boundaries (inferred winter-spring transitions) marked by step-wise change in X-ray attenuation (white-to-black icons) are shown as vertical dashed lines. Delamination (BREAK) in dentin sequence occurs at numbered increment boundary 40. Black plot between points shows pattern of change in second-order thickness. Lighter gray curve is a five-point moving average over original data. Death (dagger) occurred fifteen fortnights after the last winter-spring boundary.

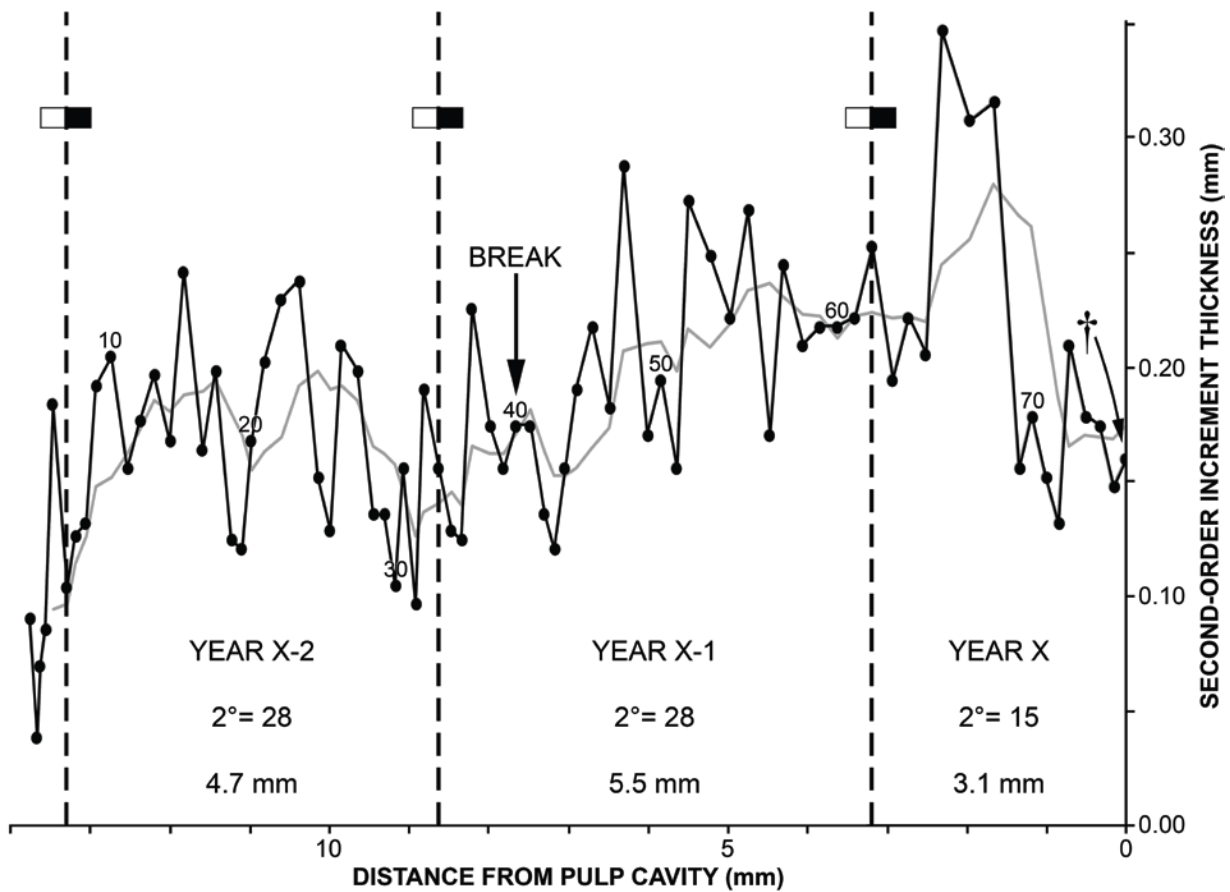


Figure 7. Close-up of polished longitudinal surface of dentin and cementum seen at far right end of Fig. 1D. Dark layer below DCJ is cementum, forming the outer surface of the tusk. Dentin extends from DCJ upward to the surface of the pulp cavity. Epoxy was poured into a chalky, delaminated zone of dentin to stabilize it prior to cutting smaller-scale sample blocks (see straight cut at left margin of this image). Asterisk within cementum layer marks location of a first-order (annual) periradicular feature distinguished by a pronounced deflection of the DCJ (seen also in Fig. 1D, lower right). Schreger features (dark-light banding here seen in longitudinal section) reflect phase shifts in undulations of dentinal tubules; these are not incremental features. Scale bar at lower left.

